Civil Engineering Beyond Limits 3 (2022) 1579
Civil Engineering Beyond Limits
journal home: www.acapublishing.com/journals/1/cebel

Research Article

Rectangular C-Device with Circular Transitions: Modelling Approaches and Development of an Equivalent Nonlinear Inelastic Spring for Seismic Analysis

Oday Al-Mamoori*,[1], J. Enrique Martinez-Rueda[2].
[1]*Al-Mustaqbal University College, Iraq*
[2]*Corresponding author, School of Architecture, Technology and Engineering, University of Brighton, UK*

Keywords

C-device,
Yield device,
Equivalent nonlinear inelastic spring,
Hysteretic energy dissipation device,
Nonlinear analysis,
Seismic retrofitting.

Abstract

Yield devices of "C" shape, known as C-devices, supplement the energy dissipation sources when installed in earthquake resistant structures. However, the explicit modelling of C-devices is time consuming. Accordingly, this paper presents a new reliable methodology to define and calibrate an equivalent uniaxial inelastic spring that effectively reproduces the expected hysteretic response of a C-device. The shape of the C-device under study resembles that of a rectangular portal frame with circular interior corner transitions to avoid stress concentration and to control the extension of the dissipative region. The characterization of the properties of the equivalent spring is supported by both, finite element (FE) analyses of a family of C-devices and by experimental validation. Two types of FE models are used to predict the response of the C-device. A simple FE model idealizes the device as an inelastic frame with pinned supports, whereas the more elaborate model analyses the device as a C-shaped inelastic plate under in-plane actions and explicitly reproduces the boundary conditions of the plate at the device connections. Results indicate that the FE analysis results and those obtained with the equivalent inelastic spring are in a good agreement with experimental tests for monotonic and reversed cyclic loading.

1. Introduction

Hysteretic energy dissipation devices (HEDDs) have been successfully developed during the last four decades as divulgated in several state-of-the-art reviews [6-9]. Among the world of HEDDs, yield devices made of mild steel have become very popular tools for seismic design or the redesign of existing structures [1-5].

Yield devices are normally designed to dissipate most of the energy input during earthquake ground motion (EGM). An early version of a C-device of rectangular cross section as shown in Fig. 1 was developed at the Physical and Engineering Laboratory in New Zealand [10]. This study showed that the device has the dual advantage of providing hysteretic damping with simple installation procedures. The device was proposed for the seismic retrofitting of a RC bridge [11]. The C-device with a yielding element of circular cross-section [12] shown in Fig. 2 was incorporated in several RC bridges. To avoid brittle response, the device was fabricated using cast steel arms connected to the steel solid beam using welding well away from the critical region of the yielding element.

An interesting variation of a C-device is the radial assembly of curved C-devices shown in Fig. 3. This assembly has been used in RC bridges in the form of dissipative connections between the bridge deck and its abutments [6]. A national survey reported in [14] found that by the end of 1991 several RC bridges were considered seismically protected by this device. Fig. 4 shows the incorporation of curved C-devices into chevron bracing. These devices are cut from a thick steel plate and work in a plane stress condition, while their geometry promotes an almost uniform plastification under small displacements.

More recently, the rectangular C-device described in [5] and shown in Fig. 5 was proposed as an alternative cheaper C-device and it was originally conceived as a key element of the dissipative bracing of low structural invasivity. Due to its simpler geometry, the C-device can be fabricated from a rectangular mild steel plate avoiding an elaborate cutting process. The C-device has an overall rectangular shape with circular interior corner transitions of radius r and a dissipative region of length L_d. The circular transitions reduce stress concentration at the interior corners and hence yielding is expected mainly within the dissipative region. Reference [5] describes a test under reversed cyclic loading of the device as an integral component of a dissipative bracing system. Although this test clearly revealed the hysteretic energy dissipation capacity of the device and the visual demarcation of the dissipative region, no detailed instrumentation was used to monitor specifically the response of the C-device and no tests were conducted on the device alone. Furthermore, the C-devices described in [5] were assumed to behave in an elastic perfectly plastic manner and no detailed FE analysis of the C-device were conducted.

Accordingly, the main objective of this paper is to study in detail the cyclic response of rectangular C-devices with circular corner transitions. This with the aim of calibrating an equivalent inelastic spring that drastically reduces the computational effort related to the inelastic modelling of the device, while reproducing the hysteretic response expected in the FE models of the C-device. To achieve the above objectives two FE analysis approaches that explicitly model the device are followed. The simpler model of the C-device considers the device as an assembly of inelastic frame elements. The more elaborate model conceives the C-device as an assembly of inelastic plate elements under plane stress. Results obtained from inelastic analyses using the above FE models and the equivalent spring are validated by experimental test results of the device under monotonic and cyclic loads.

*Corresponding Author: osama_amer@cu.edu.eg
Received 08 December 2021; Revised 30 August 2022; Accepted 31 August 2022 https://doi.org/10.36937/cebel.2022.1579

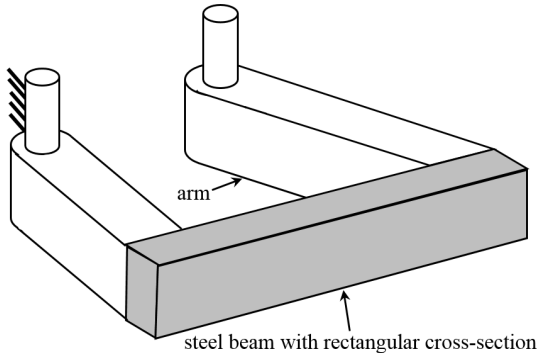

Figure 1. C-device of rectangular cross section [10]

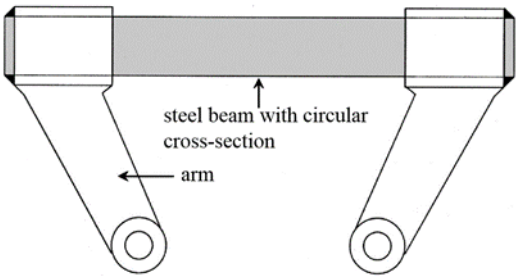

Figure 2. C-device of circular cross-section [12,7]

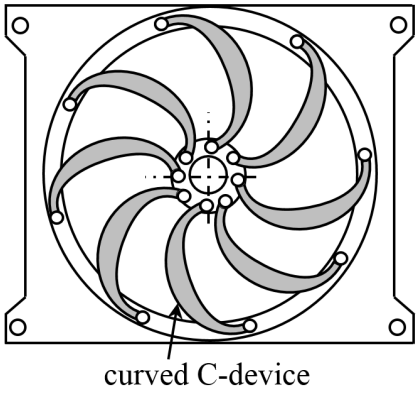

Figure 3. Assembly of curved C-devices [6]

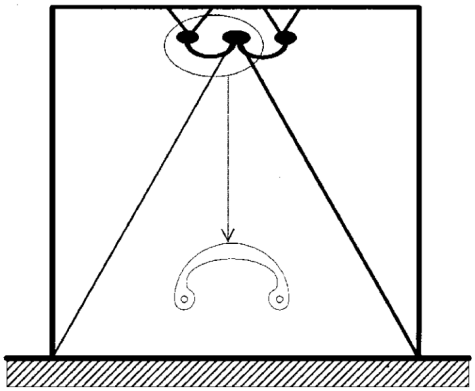

Figure 4. Application of curved C-device [17,7]

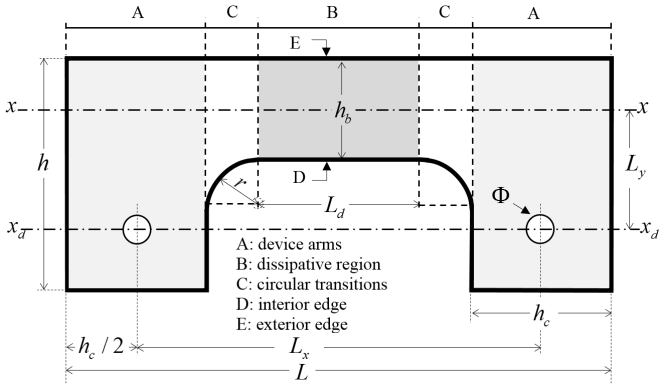

Figure 5. Simple C-device with circular transition at interior corners [5]

2. Study of the C-device idealized as an inelastic frame

2.1. Geometry of the devices

To assess the effect that L_d, r and the aspect ratio h_b/L_d of the dissipative region have on the performance of the C-device, a number of FE models using inelastic fibre frame elements were initially studied. SAP2000 [19] was used for these analyses.

Table 1. Dimensions of models (refer to Fig. 5)

Device Code	L_d [mm]	r [mm]	h_b [mm]	h_c [mm]	L_y [mm]	L [mm]	L_x [mm]	h [mm]	Ø [mm]
R90-0.80h_b	140	90	175	240	206	800	560	400	50
R90-1.37h_b	240	90	175	240	206	900	660	400	50
R90-1.60h_b	280	90	175	240	206	940	700	400	50
R100-0.8h_b	140	100	175	240	206	820	580	400	50
R100-1.37h_b	240	100	175	240	206	920	680	400	50
R100-1.60h_b	280	100	175	240	206	960	720	400	50
R110-0.80h_b	140	110	175	240	206	840	600	400	50
R110-1.37h_b	240	110	175	240	206	940	700	400	50
R110-1.60h_b	280	110	175	240	206	980	740	400	50

Table 1 summarizes the dimensions of the family of C-devices. All devices are assumed to have been cut from a steel plate 10mm thick.

2.2. FE model of the C-device using frame elements

The device was conceived as an assembly of the 3 regions identified in Fig. 5 as:

- Device arms – these regions were modelled using rigid links.
- Circular transitions – these regions were modelled by 20 nonlinear inelastic fibre elements with rectangular cross sections of variable depth.
- Dissipative region - modelled by 5 nonlinear inelastic fibre elements with constant cross section. Convergence studies showed there was no need to refine the FE mesh further.

The above fibre elements refer to standard frame elements available of SAP2000 that incorporate potential plastic hinges at the end of the elements. The behavior of these hinges is characterized based on the explicit inelastic behavior of the material properties of the steel contained in a number of regions (i.e. fibres) in which the cross section is discretized. For the inelastic regions, 30 fibres were used to model the rectangular cross section of the frame elements. Fig. 6 shows the simplified model of the C-device. The C-device was modelled using an assembly of 45 inelastic fibre elements. Steel was modelled using its

cyclic curve as the backbone of its hysteretic loops assuming kinematic hardening. The yield strength of steel was taken as 275 MPa. The parameters of the cyclic curve of steel K' and n' were estimated based on parameters of the monotonic stress-strain curve (e.g. steel model shown in [20]). The cyclic curve of steel was estimated based on the equation suggested in [22] given below

$$\sigma_s = K'\left(\varepsilon_p\right)^{n'} \quad (1)$$

where σ_s and ε_p are the normal stress and plastic strain, respectively.

The cyclic yield strength f'_y and the cyclic yield strain ε'_y for mild steel were taken as 206 MPa and 0.001031, respectively. These values were estimated from normalized experimental stress-strain curves of steel for yield strength of 383 MPa, yield strain of 0.001433 and ultimate strength of 400 MPa [23]. Consequently, the parameters n' and K' of the cyclic curve were estimated to be 0.12 and 476 MPa respectively.

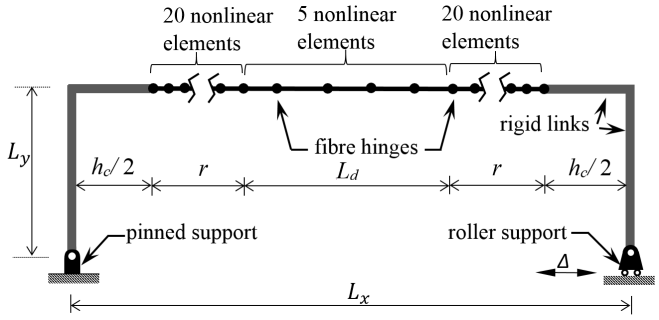

Figure 6. FE mesh of C-device idealized as an inelastic frame

2.3. Monotonic response of C-devices

Fig.7 shows an example of the influence of the dissipative region length L_d on the tensile monotonic response of the C-device. In general, the shorter the length of the dissipative region the higher the strength of the device. However, the difference in strength is not significant. In fact, a 3% average maximum difference was identified.

A clearer picture of the overall behavior of the C-devices can be established in terms of the relationship aspect ratio of dissipative region vs. maximum device strength. Fig. 8 compares the strength of the device at maximum displacement for the family of devices. It is observed that the smaller the radius of circular transition the higher the strength of the device. However, the differences in device strength seem insignificant (maximum difference in the range of 3.5kN).

Table 2 summarizes the monotonic response of the family of C-devices in terms of maximum device strength P_{max}, yield strength P_y, yield displacement Δ_y, displacement at maximum strength Δ_u, yield stiffness K_y and displacement ductility demand μ_Δ. The yield strength and the yield displacement were obtained based on the yield criterion defined in [24]. Results show that Δ_y decreases for increasing values of L_d. Hence, for the same device deformation, the displacement ductility demand increases for decreasing dissipative region lengths. It is evident that device $R100\text{-}1.37h_b$ exhibits the largest yield stiffness.

In all the preliminary analyses described above P-delta effects have been neglected. However due to the shape of the device these effects can play a significant role under large deformations. For instance, for devices working in compression Fig. 9 illustrates the importance of accounting for P-delta effects. In fact, the model neglecting the P-delta effect fails to predict the deformation softening of the device at large deformations. On the other hand, the consequences of the P-delta effect are different depending on the device working either in tension or in compression as illustrated in Fig. 10, which indicates that under tension the strength of the device does not drop whereas under compression at large deformations the device shows strength drop leading to deformation softening. Therefore, it is anticipated that a refined calibration of the equivalent inelastic spring may include asymmetry of response; hence the backbone curve for tension may be different for that under compression.

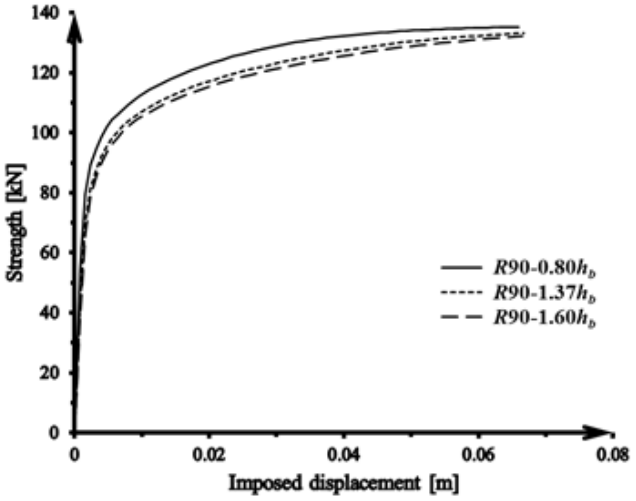

Figure 7. Influence of L_d on the monotonic behaviour of the C-device under monotonic tensile loading.

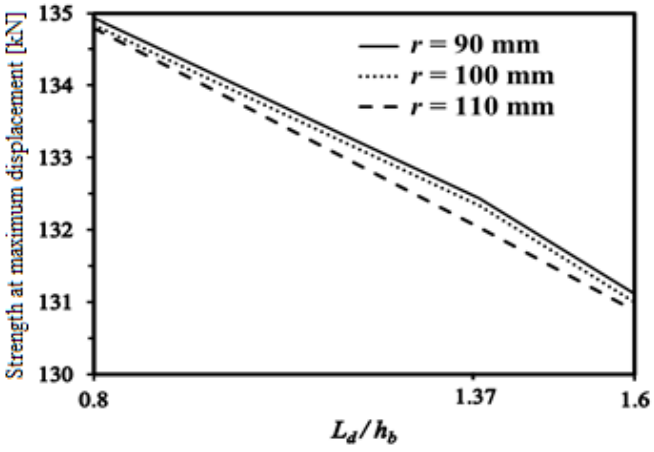

Figure 8. Relationship between the aspect ratio of the dissipative region and the device strength for different radii of the circular transition (devices acting in tension).

Table 2. Summary of parameters of tensile monotonic responses obtained by analysis

Device code	P_{max} [kN]	P_y [kN]	Δ_y [mm]	Δ_u [mm]	K_y [kN/m]	μ_Δ
$R90\text{-}0.80h_b$	134.9	54	0.0020	0.066	27,076	33.00
$R90\text{-}1.37h_b$	132.4	41	0.0021	0.066	21,247	31.44
$R90\text{-}1.60h_b$	131.1	38	0.0025	0.066	20,672	26.40
$R100\text{-}0.8h_b$	134.8	53	0.0018	0.066	15,039	37.71
$R100\text{-}1.37h_b$	132.3	40	0.0020	0.066	30,014	33.00
$R100\text{-}1.60h_b$	131.0	37	0.0023	0.066	20,127	29.33
$R110\text{-}0.80h_b$	134.7	51	0.0018	0.066	16,298	37.71
$R110\text{-}1.37h_b$	132.0	39	0.0020	0.066	29,160	33.00
$R110\text{-}1.60h_b$	130.8	36	0.0025	0.066	19,636	26.40

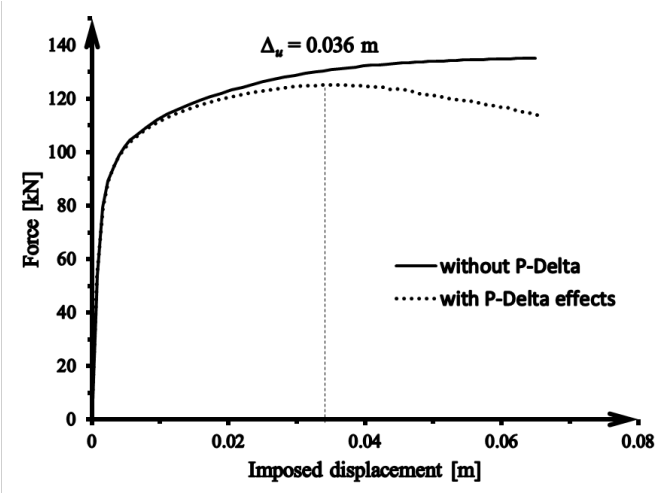

Figure 9. Influence of P-Delta effect on the compressive response of C-device R90-0.80hb.

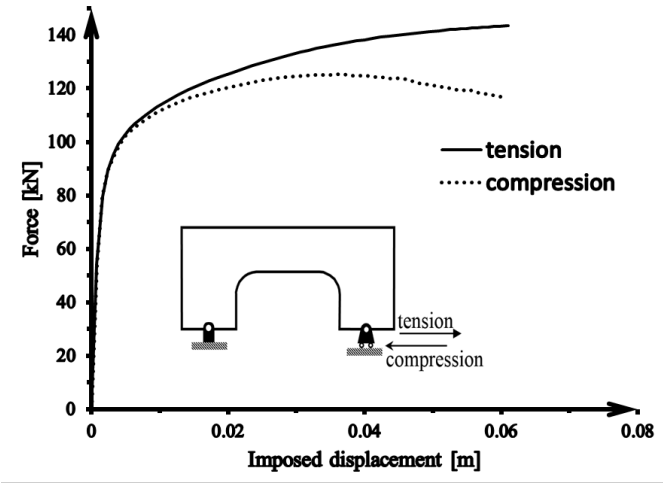

Figure 10. Comparison example of pushover responses for device $R90\text{-}0.80h_b$ working under tension or compression (P-Delta effects considered).

2.4. Modelling C-devices using equivalent nonlinear inelastic springs

To model the nonlinear behaviour of the C-device in a simpler way, a single nonlinear inelastic spring with kinematic hardening can be used for each device installed in a structure. The pushover response obtained using a more detailed FE model of the device (e.g. Fig. 6) can be used to define the properties of the equivalent spring. The kinematic hardening model is an appropriate model for steel members as effectively simulates cyclic multi-nonlinear plasticity. The equivalent nonlinear spring is simply delimited by two nodes as illustrated in Fig. 11.

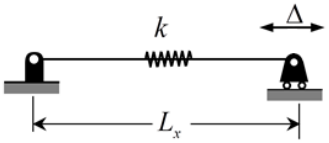

Figure 11. Sketch of the equivalent nonlinear spring.

3. Response under reversed cyclic loading

A comparison of the cyclic response of the C-device predicted by the frame model (described in section 2.2) and the equivalent spring has been established. The analysis was conducted by imposing the displacement-controlled load history shown in Fig. 12a.

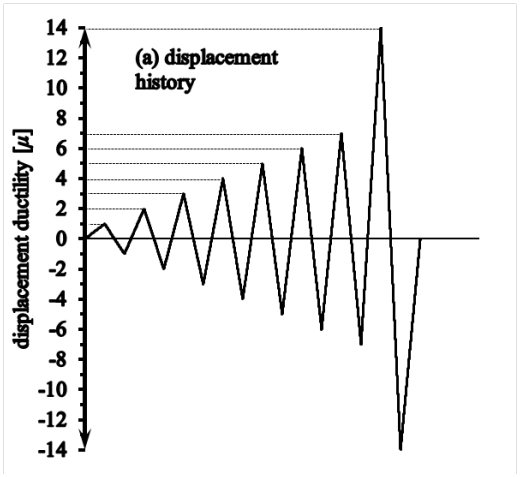

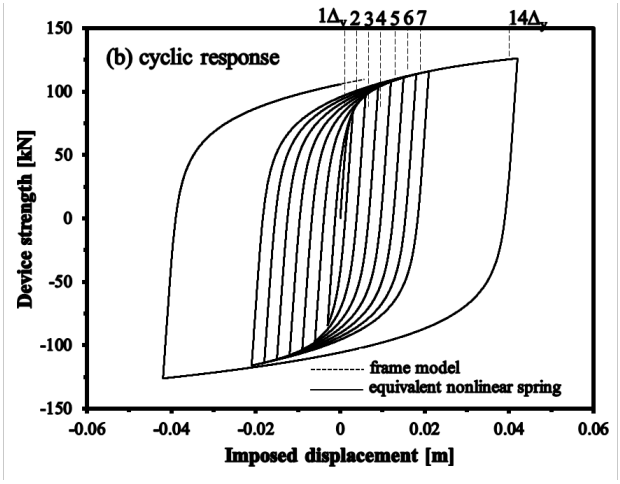

Figure 12. Displacement history and comparison of cyclic response for a C-device $R90\text{-}1.6h_b$ using two different modelling approaches.

As shown in Fig. 12b, the hysteretic behaviour of the frame model of the C-device $R90\text{-}1.6h_b$ (see Table 1) is virtually the same as that of the equivalent nonlinear inelastic spring model. However, there is a clear difference in computational effort required for the models. For instance, the spring model makes use of a single inelastic element whereas the frame model requires 45 inelastic fibre elements and each of these elements contains 2 potential plastic hinges characterized by 30 fibres each. Fig. 12b also confirms that the force resisted by the device depends on the imposed ductility. It can be seen for instance that under a displacement of $14\Delta_y$, the force developed by the C-device is approximately 30% greater than the yield strength obtained from the monotonic response. Due to the excellent matching of cyclic response between the two models the evolution of hysteretic energy and stiffness degradation are also well predicted by the equivalent spring as confirmed by Fig. 13 and 14.

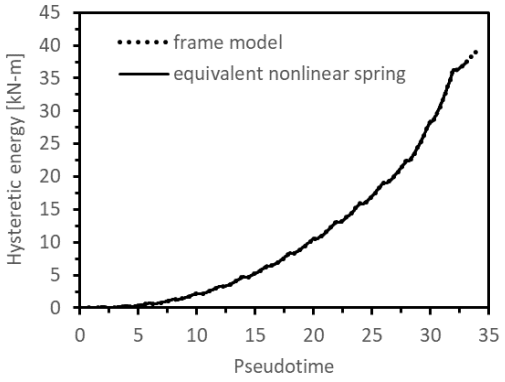

Figure 13. Comparison of the hysteretic energy dissipated under reversed cyclic loading by the C-device for two different modelling approaches.

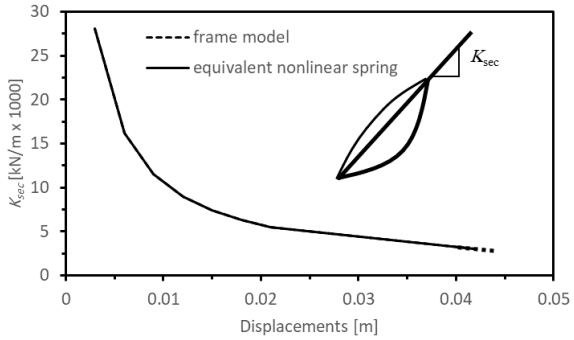

Figure 14. Comparison of predicted device stiffness degradation under reversed cyclic loading for two different modelling approaches.

4. Modelling of the C-device as installed into an RC member

4.1. Definition of member models

One of the intended new applications of the C-device is for the seismic retrofit of precast concrete structures [21]. A pinned connection in this type of construction can be enhanced by connecting a C-device between the members converging at the connection. Fig. 15 shows an RC column model including two different approaches to model the incorporation of C-devices. The column supports a lumped mass M which was selected so that the initial period of the system is 0.4sec. As the column is pin-jointed at its base the attached devices are the main sources of lateral strength and stability of the system.

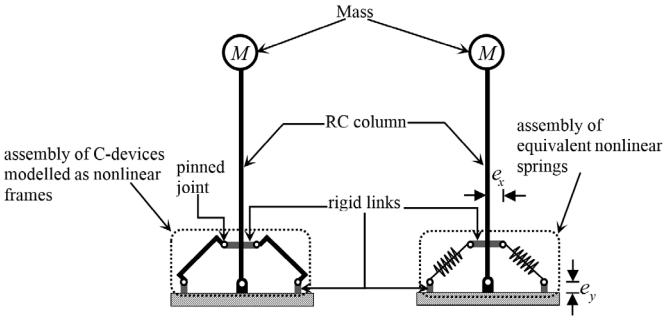

Figure 15. Incorporation of C-devices around a pinned column base.

A set of rigid links with length equal to half of the column cross section depth (see Fig. 16) is used to connect the devices to the column. Two additional rigid links connect the devices to the foundation. The assembly of connection plates (consisting of anchor bolts and base plates with pinned joints) shown in Fig. 16 must have adequate strength and stiffness to ensure the maximum efficiency of the C-devices. The assembly must be designed to resist forces higher than the maximum force anticipated in the devices. This with the aim of concentrating energy dissipation only in the devices while avoiding yielding of the connecting elements [25]. The RC column was modelled by inelastic frame elements and a fibre element approach was used to predict the response of its plastic hinge regions. More detailed information about this model is given elsewhere [21].

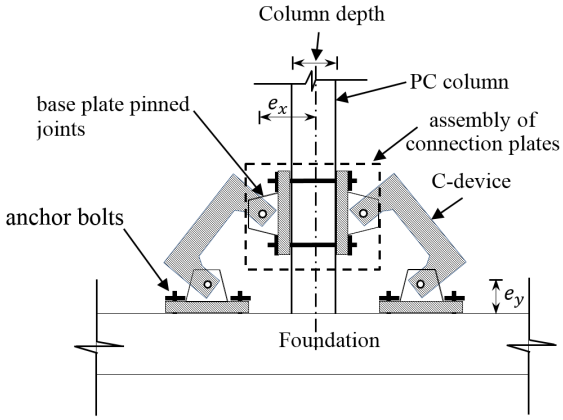

Figure 16. Connection between device and column.

4.2. Response Under Monotonic Lateral Loading

The pushover responses of the columns of Fig. 15 are illustrated in Fig. 17. These responses were obtained by applying lateral displacements at the top of the column. The yield displacement and maximum strength of the column model using C-devices R90-1.6h_b (refer to Table 1) were found to be 0.011m and 123.0 kN respectively. Very close agreement between the two pushover responses under comparison can be observed.

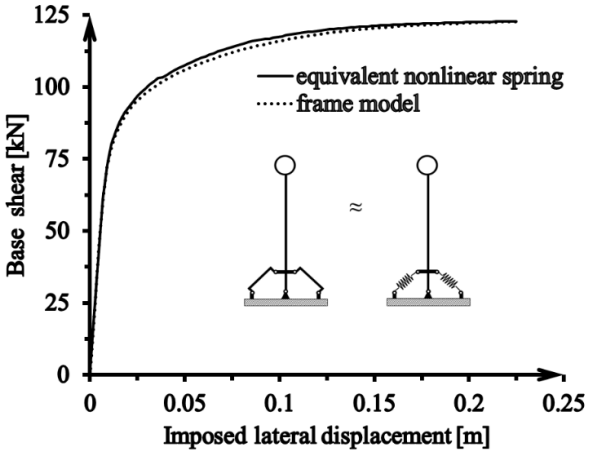

Figure 17. Comparison of pushover response of the cantilever column with C-devices.

4.3. Response under harmonic excitation

The dynamic response of the columns of Fig. 15 under harmonic excitation with viscous damping neglected was also studied. For simplicity, the excitation (see Fig. 18a) was assumed to have 0.5gm/sec^2 amplitude, frequency of excitation Ω = 15.7rad/sec and duration of 2sec; where g is the acceleration of gravity. On the other hand, the vibration frequency of the system based on its elastic stiffness is ω = 15.5rad/sec.

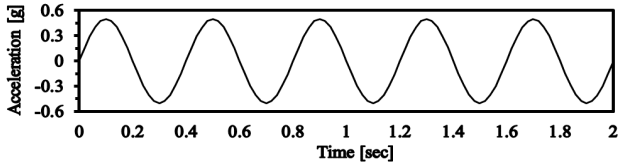

(a) harmonic excitation of short duration.

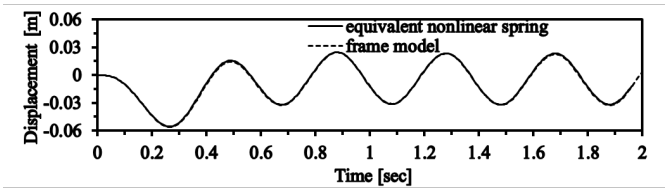

(b) displacement response.

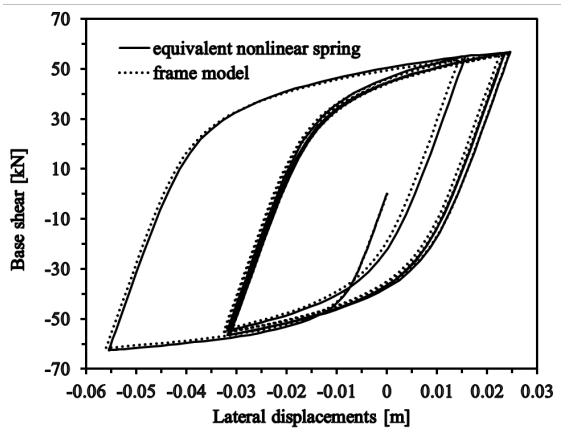

(c)Hysteretic response

Figure 18. Comparison of dynamic response under harmonic excitation for a cantilever column.

Fig. 18b shows the displacement responses of the 2 column models under comparison. Excellent agreement can be observed between the two responses, both in terms of amplitude and phase. Good agreement in hysteretic responses is also observed as illustrated in Fig. 18c.

4.4. Response under earthquake ground motion

Nonlinear time-history analyses of the column models of Fig. 15 under the action of the El Centro 1940, NS earthquake record were also performed neglecting viscous damping effects. To estimate the effect of residual displacements the analyses considered only the first 12 seconds of the EGM adding 5 seconds of zero acceleration as shown in Fig. 19. Using amplitude scaling, three intensities were considered: 100% intensity (PGA = 0.32g), 200% intensity (PGA = 0.64g), and 300% intensity (PGA = 0.96g). The first intensity is representative of EGM that may initiate yielding in the devices. The second and third intensities are representative of EGMs that produce significant yielding in the devices.

Fig. 20 indicates that, irrespectively of the EGM intensity, both models have virtually the same displacement response. The maximum displacement for both models is -0.037m, -0.093m and -0.18m for EGM scaled to PGA = 0.32g, 0.64g and 0.96g, respectively. As expected, the greater the EGM intensity the larger the residual displacements are. Also, as shown in Fig. 21, the predicted hysteretic responses show very close agreement between them, both in terms of strength and stiffness evolution.

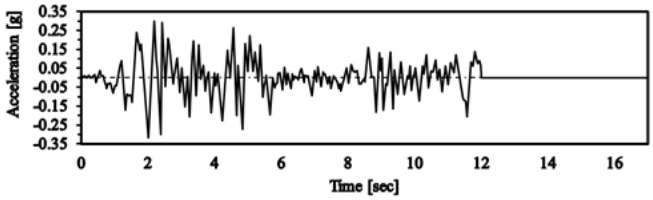

Figure 19. El Centro NS 1940 EGM (first 12 sec)

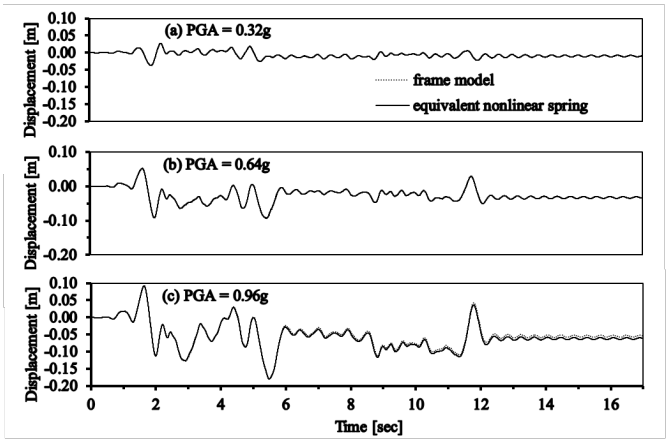

Figure 20. Displacement response of the column with C-devices for two different device models under El Centro EGM scaled at 3 intensity levels.

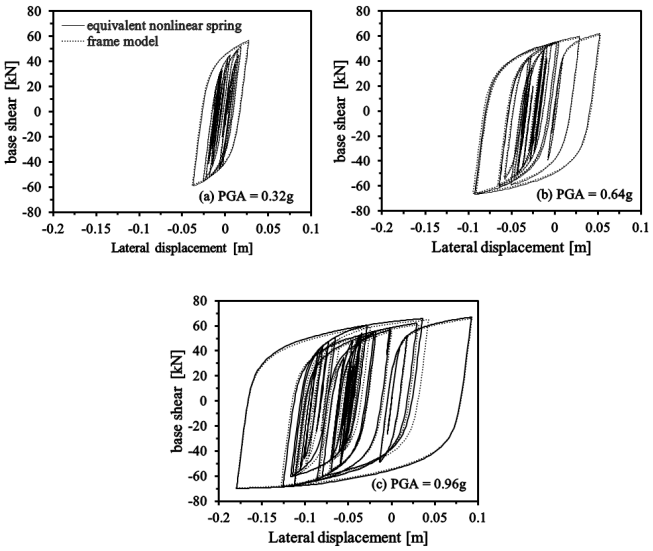

Figure 21. Hysteretic behaviour of cantilever column with C-devices for two different device models under scaled El Centro EGM

5. Study of the C-device modelled as an assembly of 2D plate elements under plane stress

5.1. Geometry and dimensions of FE models and response under monotonic loads

FE analyses of the C-device using 2D plate elements under plane stress were also conducted using the computer code ADINA [26]. Other researchers [27-30] have followed similar FE idealizations to simulate the response of steel members in detail. The adopted mesh of 2D plate elements (10mm thick) under plane stress is shown in Fig. 22. This elaborate FE model was meshed using 8-node quadrilateral finite elements. To identify whether the mesh used is fine enough, the criterion of the stress band method [27] was applied. The FE model also

accounts for the frictional forces developed at the interface between the steel plate conforming the C-device and the bolts used to pin-join the device to its base plates. The approach to model this frictional interaction is based on assuming that plate elements are selected to be the 'contactor' (deformable surface) and the bolt is defined as a rigid surface. Additionally, within the contact pair, the nodes of the device elements are prevented from penetrating the segments of the bolt surface but not vice versa. A closed gap was assumed at the contact surface, which means that the device elements are idealized as touching the bolt surface at the start of the analysis. A friction coefficient equal to 0.4 [29] was assigned within the contact elements. Finally, the same cyclic curve for steel used in Section 2.2 was also adopted.

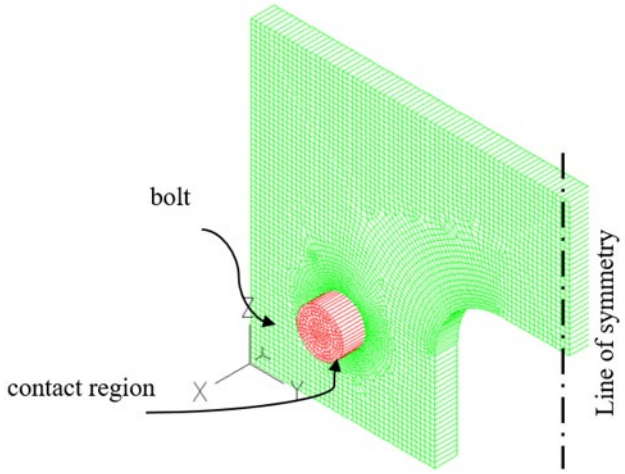

Figure 22. FE mesh of the C-device elaborate model

Fig. 23 shows an example of a comparison between the pushover responses of the device modelled as either an inelastic plane frame or as an assembly on inelastic plate elements. Very good agreement is observed between the models in terms of strength and stiffness for the entire range of displacements. The effect of friction on device response predicted by the elaborate FE model is summarized in Fig. 24. As expected, higher device forces are developed when friction is accounted for. However, on the average, accounting for friction only results in a very mild increase of forces in the order of 6%.

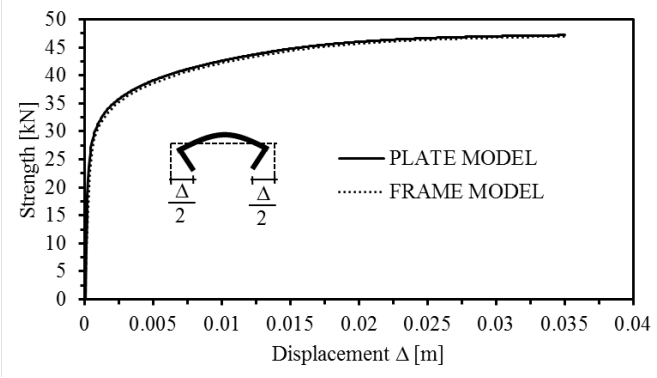

Figure 23. Comparison of a FE analysis predictions for device $R90\text{-}1.6h_b$.

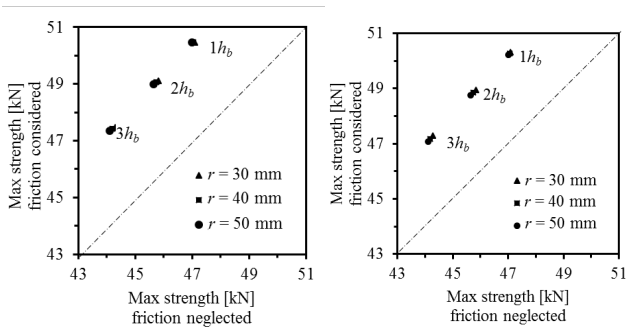

Figure 24. Comparison of predicted device strength, with and without friction, monotonic loads for different radii of the circular transition and different lengths of the dissipative region

5.2 Distribution of Von Mises stress

Several device specimens with dimensions summarized in Table 3 were fabricated and tested in the laboratory. The FE analysis of the specimens are discussed here. As exemplified in Fig. 25 stress concentration occurs around the circular hole where the bolt and device interact. In fact, there is a region around the bolt where the bearing stress may induce localized yielding in the device. However, the extension of this region is too small to have a negative effect on the performance of a well-designed device.

Table 3. Dimensions of C-devices tested (refer to Fig.5)

Device code	L_d [mm]	r [mm]	h_b [mm]	h_c [mm]	L_y [mm]	L [mm]	L_x [mm]	h [mm]	Ø [mm]
$R30\text{-}1h_b$	58	30	58	80	65	278	198	130	20
$R30\text{-}2h_b$	116	30	58	80	65	336	256	130	20
$R30\text{-}3h_b$	174	30	58	80	65	394	314	130	20
$R40\text{-}1h_b$	58	40	58	80	65	298	218	130	20
$R40\text{-}2h_b$	116	40	58	80	65	356	276	130	20
$R40\text{-}3h_b$	174	40	58	80	65	414	334	130	20
$R50\text{-}1h_b$	58	50	58	80	65	318	238	130	20
$R50\text{-}2h_b$	116	50	58	80	65	376	296	130	20
$R50\text{-}3h_b$	174	50	58	80	65	434	354	130	20

Fig. 25 also suggests that the use of a generous circular transition is effectively keeping most of the yielding within the dissipative region. In fact, the Von Mises stress distribution shows the most intense inelastic values mainly over a large volume of the dissipative region. Nevertheless, mild yielding is evident over a small region of the circular transition.

The above findings confirm the effectiveness of the circular transition adopted in the geometric design of the device.

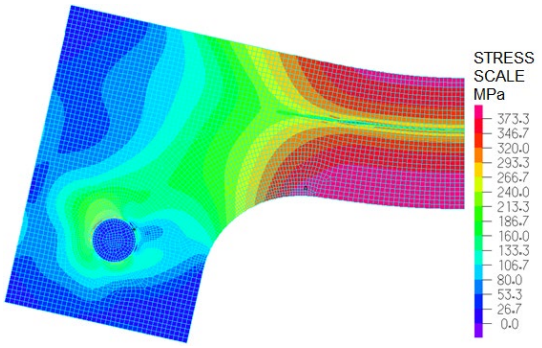

(a) C-device R40-2hb subjected to tension load

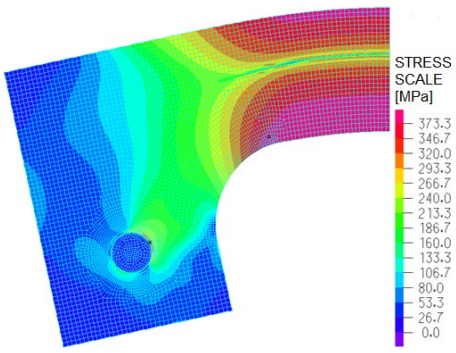

(b) C-device $R40\text{-}2h_b$ subjected to compression load

Figure 25. Predicted von Misses stress distribution in C-device $R40\text{-}2h_b$ (friction considered)

6. Test results vs. numerical models of the C-device

Comparisons between experimental and numerical results obtained from both, the plane frame model and the plate model of the device are discussed in this section. In the interest of brevity only one example is given for both models. An exhaustive set of results is given elsewhere [21].

The experimental results reported here correspond to devices *R*30-1h_b, *R*30-2h_b, *R*50-1h_b and *R*50-2h_b with dimensions given in Table 3. These devices were cut from a grade S275 mild steel plate 10mm thick. The cyclic tests were conducted based on the loading protocol described in [31]. Strain rate effects were avoided following the guidance extracted from [32].
A total of 16 specimens were tested under monotonic and cyclic loads using a strain rate of 2.5x10^{-6}/sec. A typical hysteresis response observed in the cyclic tests is exemplified in Fig. 26. The observed cyclic performance of the specimen reveals stable hysteretic behaviour with no signs of stiffness or strength degradation. This confirms the adequacy of the aspect ratios adopted for the geometric design of the devices.

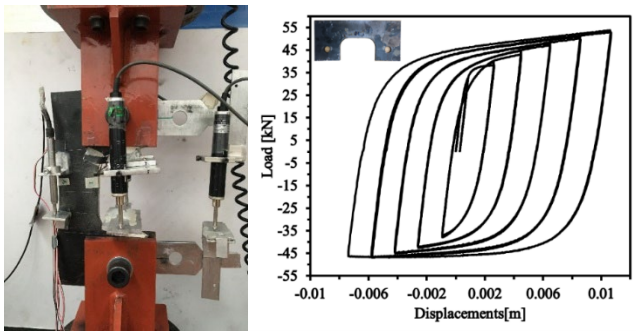

Figure 26. Hysteretic response of C-device R30-1hb

6.1. Test results vs. frame model predictions

Fig. 27 shows an example of the comparison between experimental results vs. numerical predictions obtained with the frame model of the device (see model in Fig. 6). It is observed that the model was robust enough to closely predict the cyclic response of the C-device. The loading and unloading stiffnesses predicted by the frame model are slightly higher than those observed in the test. The strengths of the specimen at small and large displacements predicted by the frame model match well the observed experimental behaviour. Based on the above comparisons it can be argued that the frame model reliably predicts the observed cyclic behaviour of the C-devices; hence, results from this model can be used with confidence to calibrate the properties of an equivalent nonlinear spring.

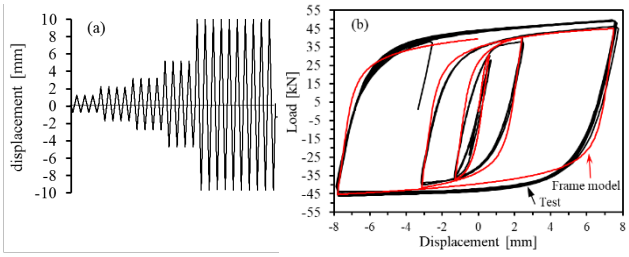

Figure 27. Applied displacement history and test vs. numerical prediction

6.2. Test results vs. plane stress plate model

Fig. 28 compares numerical results predicted by the plate model with experimental observations under monotonic loading. This figure suggests that this model can successfully predict the observed experimental behavior. There is good agreement between the predicted and the observed deformed shapes. Also, the plate model effectively captures the expected stress distribution as inelastic stresses are mainly contained across the dissipative region of the device while stresses in the circular transition regions are relatively low (mild yielding is evident across a small portion of these regions). Similar agreements were also observed with the other tests [21]. The above observations confirm that the intended effect of the circular transitions adopted in the original intuitive geometric design of the C-device [5] actually occurs, i.e. yielding is effectively controlled to take place primarily inside the dissipative region. In fact, the Von Mises stress distribution presents the most intense inelastic values mainly over a large volume of the dissipative region.

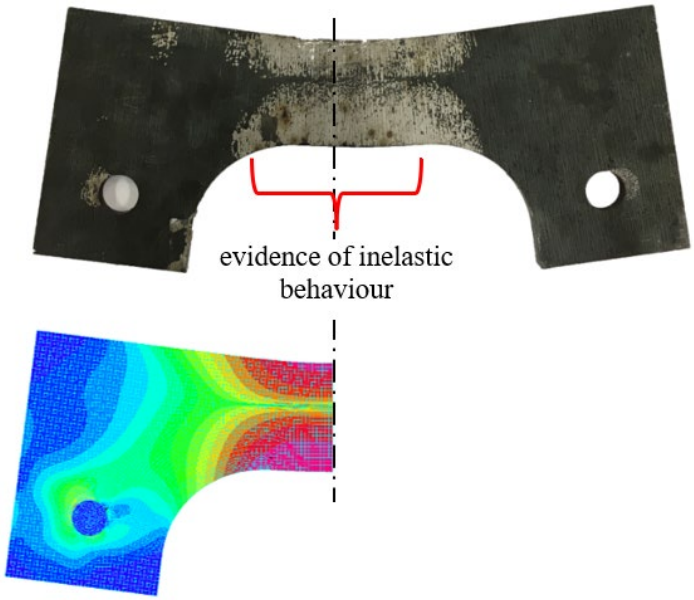

Figure 28. Predicted distribution Von Mises stress and observed distribution of strains for device R50-1hb subjected to monotonic load.

7. Conclusions

In this work, a rectangular C-device with circular corner transitions has been studied using explicit FE models for two different levels of sophistication. Results from these analyses have been used to calibrate the properties of an equivalent nonlinear inelastic spring that can handle the effective modelling of the device in a much simpler and efficient manner. The simpler FE model is a 2D frame inelastic model, whereas the more elaborate model is an inelastic 2D plane stress model. Several FE analyses using these models have been presented and compared both, with experimental results and with predictions obtained with the equivalent spring. These comparisons showed that both FE models effectively reproduce the monotonic and cyclic responses of the device. FE model results confirmed that the adoption of circular transitions at the interior corners of the device have a positive effect on the performance of the device by controlling the location of yielding to be contained inside the prescribed dissipative region of the device. Based on the above results and observations it is concluded that:

The use of equivalent nonlinear inelastic springs is an effective practical approach to model the monotonic and cyclic behavior of the C-devices that lead to significant savings of computing effort. Hence there is no need to use FE models to simulate each of the C-devices.

The properties of these springs can be calibrated based on the results obtained from either reliable inelastic FE analysis or tests of the C-device.

The concept of equivalent nonlinear springs described in this paper has been used by the authors as an efficient tool to study the application of C-devices for the seismic upgrading of precast concrete structures [21, 34, 35]. It is suggested that the methodology described

here for the calibration of the equivalent springs can be also applied to other types of C-devices.

Acknowledgments

The first author would like to thank the Iraqi Ministry of Higher Education and Scientific Research and the Babylon University in Iraq for sponsoring his PhD studies at the University of Brighton, U.K.

Declaration of Conflict of Interests

The authors declare that there is no conflict of interest. They have no known competing financial interests or personal relationships that could have appeared to influence the work reported in this paper.

References

[1.] Whittaker, A.S., et al., Seismic testing of steel plate energy dissipation devices. Earthquake Spectra, 1991. 7(4): p. 563-604.

[2.] Perry, C.L., et al., Seismic upgrade in San Francisco using energy dissipation devices. Earthquake Spectra, 1993. 9(3): p. 559-579.

[3.] Tsai, K.-C., et al., Design of steel triangular plate energy absorbers for seismic-resistant construction. Earthquake spectra, 1993. 9(3): p. 505-528.

[4.] Martinez-Rueda, J.E. Incorporation of hysteretic devices on bracing systems of low invasivity. A new approach for the seismic redesign of framed structures. Proceedings of the 12th World Conference on Earthquake Engineering, New Zealand, 2000.

[5.] Martinez-Rueda, J.E. Cyclic response of a low invasivity bracing system for the passive control of framed structures. Proceedings of the 13th World Conference on Earthquake Engineering, Canada, 2004.

[6.] Skinner, R.I., W.H. Robinson, and G.H. McVerry, An introduction to seismic isolation. 1993: John Wiley & Sons.

[7.] Martinez-Rueda, J.E., On the evolution of energy dissipation devices for seismic design. Earthquake Engineering Research Institute, 2002. 18(2): p. 309-346.

[8.] Soong, T. and B. Spencer, Supplemental energy dissipation: state-of-the-art and state-of-the-practice. Engineering Structures, 2002. 24(3): p. 243-259.

[9.] Symans, M.D., et al., Energy Dissipation Systems for Seismic Applications: Current Practice and Recent Developments. Journal of Structural Engineering, 2008. 134(1): p. 3-21.

[10.] Kelly, J.M., R. Skinner, and A. Heine, Mechanisms of energy absorption in special devices for use in earthquake resistant structures. Bulletin of NZ Society for Earthquake Engineering, 1972. 5(3): p. 63-88.

[11.] Skinner, R., A. Heine, and R. Tyler. Hysteretic dampers to provide structures with increased earthquake resistance. Proceedings of the 6th World Conference on Earthquake Engineering, New Delhi. 1977.

[12.] Skinner, R., R. Tyler, and A. Heine. Steel beam dampers for increasing the earthquake resistance of structures. Proceedings of the 7th World Conference on Earthquake Engineering, Turkey. 1980.

[13.] Skinner, R., et al., Hysteretic dampers for the protection of structures from earthquakes. Bulletin of the New Zealand National Society for Earthquake Engineering, 1980b. 13(1): p. 22-36.

[14.] Medeot, R. and L. Albajar, The evolution of seismic devices for bridges in Italy. Proceedings of the 10th World Conference on Earthquake Engineering, 1992. 4: p. 2227.

[15.] Marioni, A., Development of a new type of hysteretic damper for the seismic protection of bridges. Special Publication, 1996. 164: p. 955-976.

[16.] du Beton, F.I., Seismic bridge design and retrofit—structural solutions. fib Bulletin, 2007. 39.

[17.] Ciampi, V., F. Paolacci, and S. Perno, Dynamic tests of a dissipative bracing system for seismic control of framed structures. WIT Transactions on The Built Environment, 1996. 23.

[18.] Guan, Z., J. Li, and Y. Xu, Performance test of energy dissipation bearing and its application in seismic control of a long-span bridge. Journal of Bridge Engineering, 2009. 15(6): p. 622-630.

[19.] CSI, Integrated finite element analysis and design of structures. Computers and Structures, Inc., Berkeley, California, USA, 2015.

[20.] Park, R. and R.A. Sampson. Ductility of reinforced concrete column sections in seismic design. in Journal Proceedings. 1972.

[21.] Al-Mamoori, O., Seismic redesign of precast portal frames using yield C-devices. PhD Thesis, University of Brighton, School of Engineering and Technology. UK, 2019.

[22.] Cofie, N.G. and H. Krawinkler, Uniaxial cyclic stress-strain behavior of structural steel. Journal of Engineering Mechanics, 1985. 111(9): p. 1105-1120.

[23.] Penelis, G.G. and A.J. Kappos, Earthquake-resistant concrete structures. 1997, London: E & FN Spon.

[24.] Wen, Y.-K., Method for random vibration of hysteretic systems. Journal of the engineering mechanics division, 1976. 102(2): p. 249-263.

[25.] Martinez-Rueda, J.E., Energy dissipation devices for seismic upgrading of RC structures. PhD Thesis, Imperial College of Science, Technology and Medicine, Civil Engineering Department. UK, 1997.

[26.] ADINA, I., Adina: A Finite Element Program for Automatic Dynamic Incremental Nonlinear Analysis. 2016, ADINA Engineering Inc.: Watertown, MA, USA.

[27.] Sussman, T. and K.-J. Bathe, Studies of finite element procedures—stress band plots and the evaluation of finite element meshes. Engineering computations, 1986. 3(3): p. 178-191.

[28.] Ghabraie, K., et al., Shape optimization of metallic yielding devices for passive mitigation of seismic energy. Engineering Structures, 2010. 32(8): p. 2258-2267.

[29.] Moradi, S. and M.S. Alam, Finite-element simulation of posttensioned steel connections with bolted angles under cyclic loading. Journal of Structural Engineering, 2015. 142(1): p. 04015075.

[30.] Jiao, Y., M. Saito, and Kohno, M., Fatigue behavior of steel slit-dampers with various shapes, Proceedings of the 16th World Conference on Earthquake Engineering, 2017: Santiago, Chile.

[31.] Mezzi, M. and A. Parducci, Seismic isolated bridges structures in Italy. Proceedings of the 10th World Conference on Earthquake Engineering, 1992. 4: p. 2199.

[32.] Restrepo-Posada, J., et al., Variables affecting cyclic behavior of reinforcing steel. Journal of Structural Engineering, 1994. 120(11): p. 3178-3196.

[33.] Tyler, R., A tenacious base isolation system using round steel bars. Bulletin of the New Zealand Society for Earthquake Engineering, 1978. 11(4): p. 273-281.

[34.] Martinez-Rueda, J.E. and Al-Mamoori, O, detailed seismic modelling of portal RC frames with precast beams connected by pocket joints at the upper column ends, Proceedings of the 5th International Conference on Earthquake Engineering, 2019: Ankara, Turkey: paper 10135.

[35.] Al-Mamoori, O. and Martinez-Rueda, J.E., Application of yield devices of low invasivity for seismic upgrading of precast portal RC frames, Proceedings of the 5th International Conference on Earthquake Engineering, 2019: Ankara, Turkey: paper 10136

How to Cite This Article

Al-Mamoori, O., and Martinez-Rueda, J.E., Rectangular C-Device with Circular Transitions: Modelling Approaches and Development of an Equivalent Nonlinear Inelastic Spring for Seismic Analysis, Civil Engineering Beyond Limits, 1(2022), 1579.
https://doi.org/10.36937/cebel.2022.1579